A FAST METHOD FOR INTERFACE AND PARAMETER ESTIMATION IN LINEAR ELLIPTIC PDES WITH PIECEWISE CONSTANT COEFFICIENTS

Alejandro Cantarero

Department of Mathematics, University of California, Los Angeles
Box 951555, Los Angeles, CA 90095-1555

Tom Goldstein

Department of Electrical Engineering, Stanford University
Stanford, CA 94305

Abstract. We present a new method for the recovery of the parameters and interface from an observed solution to embedded interface linear elliptic PDEs with piecewise constant coefficients. Our approach uses the linear nature of these equations to derive a function that is approximately equal to the coefficients across the entire domain. We are then able to recover the coefficients using split Bregman implementations of standard piecewise constant segmentation methods. This results in an approach that can recover both the coefficients and the interface from the observed data incredibly quickly, allowing us to run at high resolutions in both two and three dimensions. The method has a single control parameter that is not difficult to set and allows us to easily recover complex geometry for the embedded interface. We demonstrate the method on Poisson's equation and linear elasticity.

1. Introduction

The problem of recovering the coefficients and interface between two regions of an embedded interface elliptic partial differential equation (PDE) from observations of a solution has many real world applications. In the case of Poisson's equation, these include areas such as electrical impedance tomography [6, 18, 57], groundwater flow / oil reservoir simulation [36, 37], and DC resistivity analysis [56]. In continuum mechanics, applications include imaging [30, 34], identifying material properties and inclusion detection [41, 54], design optimization [1, 5, 11, 55], and medical applications [43, 48, 51]. In medical imaging applications, the solution of this problem could potentially lead to the determination of different tissues in a patient via minimally invasive methods ([43] and references therein). The elastic material properties of tissue, muscle, and bone that are in contact are examples where the data can be well approximated by piecewise constant coefficients. However, the specific values of these coefficients will vary from patient to patient. The ability to identify these coefficients accurately for individual patients could be used to fine tune simulations, [52], allowing for improved treatment tied to a specific patient.

In some cases, only the coefficients are of interest, in others just the interface, and in some both, depending on the application area. For many of the applications discussed above, it is reasonable to assume that the coefficients are either piecewise constant or well approximated by piecewise constant functions. In the following section, we will discuss previous work that solves the parameter estimation problem (coefficients only), inverse geometric problem (interface only),

Key words and phrases. Inverse problems, elliptic problems, inverse parameter estimation, inverse geometric problems, split Bregman, image segmentation.

Email addresses: cantarer@math.ucla.edu (Alejandro Cantarero), tagoldst@stanford.edu (Tom Goldstein).

The first author is supported by the National Science Foundation under grants DMS-0502315, DMS-0652427, CCF-0830554, by UC Lab Fees Research Grant DOE 09-LR-04-116741-BERA, and the Office of Naval Research under grants ONR N000140310071, and ONR N000141010730.
The second author is supported by the National Science Foundation Post-Doctoral Fellowship program under grant NSF 08-582.

or both simultaneously. We then present a new, fast, non-variational approach to recovering the coefficients and the interface between the two regions from solution data to elliptic PDEs. We demonstrate how to compute a function that is approximately equal to the piecewise constant function we wish to solve for from a given solution to an elliptic PDE in §3. A discussion of piecewise constant segmentation methods is included in §4, which we use to find the location of the interface and determine the values of the coefficients. Finally, we demonstrate our algorithm on examples coming from Poisson's equation and linear elasticity in §5.

2. Previous Work

Variational models are very commonly used to solve the parameter estimation problem for elliptic PDEs. For Poisson's equation, some combination of output-least-squares, equation error, and the augmented Lagrangian method have been used by many authors to recover the unknown coefficients from given solution data [4, 13, 17, 23, 31, 39]. Generally, these approaches discretize the coefficients over the entire domain, rather than directly using the fact that the coefficients will only take on a small, finite number of values. This results in a need to solve for the coefficients over the entire domain and requires some kind of regularization on the coefficients. Common choices of regularizers are either total variation or Tikhonov-type. These approaches can also be applied to the equations of linear elasticity to find the Lamé coefficients [21, 33]. Approaches have also been proposed to solve only for the shear modulus [47]. Some authors have also demonstrated methods with examples applied to parameter estimation for both Poisson's equation and linear elasticity [22, 23].

The recovery of an interface contained within a computational domain has also been studied by many authors, as it has applications in such areas as determining locations of discontinuities in conductivity [29], inverse problems involving obstacles [8, 53], and optimal shape design [1]. The equations that the data are generated from vary depending on the application, but include Poisson's equation [8, 27, 29, 40] and elasticity [1, 3, 9] which are the focus of this work, as well as other elliptic problems [28, 38]. Most modern approaches use the level set method of Osher and Sethian [49] to represent the interface, due to its many nice properties, including the automatic handling of topological changes [2, 3, 8, 9, 32, 50, 53, 60]. In more recent work, some authors have simultaneously solved for both the coefficients and the interface [14, 19, 59, 26, 46, 58], rather than only solving the parameter estimation problem or the inverse geometric problem.

3. Problem Formulation

Let $\Omega \subset \mathbb{R}^d$ be open and bounded with a smooth or piecewise smooth boundary, $\partial\Omega$. We then divide Ω into two disjoint open sets, Ω_1 and Ω_2, as shown in Figure 1. The interface between the two regions will be denoted by Γ. We now look at linear elliptic PDEs with an embedded interface Γ where the coefficients of the equation are piecewise constant in the two regions delineated by Γ.

3.1. Poisson's Equation.

We first consider Poisson's equation,

$$\begin{cases} -\nabla \cdot (\beta \nabla u) = f, & \text{in } \Omega, \\ u = g, & \text{on } \partial\Omega \end{cases} \tag{1}$$

where

$$\beta = \begin{cases} \beta_1 & \text{in } \Omega_1, \\ \beta_2 & \text{in } \Omega_2 \end{cases} \tag{2}$$

with $\beta_1, \beta_2 \in \mathbb{R}$ and both positive.

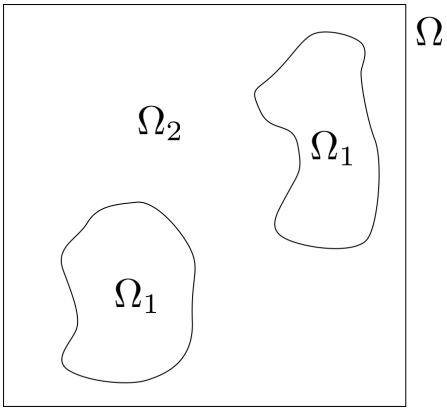

FIGURE 1. Our simulation domain, divided into two regions Ω_1 and Ω_2.

Given a solution to the above equation, u_d, as well as the associated boundary data, g, and a non-zero right-hand side f, we wish to recover the unknown coefficients β_1 and β_2 as well as the location of the interface between the regions Ω_1 and Ω_2. To accomplish this, we consider the following function defined on Ω,

$$h_{pe} = -\frac{f}{\Delta(S * u_d)} \tag{3}$$

where S is some type of smoothing operator. The smoothing operator is added at this step since the solution u_d is only guaranteed to have zero or one continuous derivatives across the interface Γ (depending on the jump conditions enforced on the interface). By first smoothing, we can then apply the Laplacian operator at all points in our domain without having to first consider if it is well-defined at that point. This step is also necessary to obtain solutions when the initial data are corrupted by noise.

We observe that the function h_{pe} is approximately equal to $\beta(x)$. Since $\beta(x)$ is a piecewise constant function, we can quickly retrieve Γ, β_1, and β_2 with any standard piecewise constant segmentation method.

3.2. **Linear Elasticity.** We also consider the embedded boundary problem with piecewise constant coefficients for linear elasticity,

$$\begin{cases} -\nabla \cdot \sigma(u) = f, & \text{in } \Omega \\ u = g_1, & \text{on } \partial\Omega_D \\ \sigma \cdot n = g_2, & \text{on } \partial\Omega_N, \end{cases} \tag{4}$$

where $\partial\Omega_D$ indicates the portion of the domain on which we specify Dirichlet boundary data and $\partial\Omega_N$ is the portion of the boundary with traction boundary conditions. The displacement u and the stress, $\sigma(u)$, are related via Hooke's law for a linear material,

$$\sigma(u) = \lambda \text{tr}(\epsilon(u))I + 2\mu\epsilon(u) \tag{5}$$

where

$$\epsilon(u) = \frac{1}{2}\left(\nabla u + \nabla u^T\right). \tag{6}$$

The Lamé coefficients describe the material properties in the two regions and are given by

$$\lambda = \begin{cases} \lambda_1, & \text{in } \Omega_1 \\ \lambda_2, & \text{in } \Omega_2 \end{cases} \qquad \mu = \begin{cases} \mu_1, & \text{in } \Omega_1 \\ \mu_2, & \text{in } \Omega_2. \end{cases} \tag{7}$$

As in the Poisson case described above, we are given a solution to this PDE, u_d, as well as the boundary data g_1 and g_2, and the external forces f, which again need to be non-zero. Given these data, we then wish to find the four Lamé coefficients as well as Γ. We proceed as before, by first smoothing the data with some smoothing operator and then plugging the function u_d into the linear elasticity operator (with no interface),

$$-h_\lambda(x)\nabla \cdot \text{tr}(\epsilon(S * u_d))I - 2h_\mu(x)\nabla \cdot \epsilon(S * u_d) = f. \tag{8}$$

where $h_\lambda(x)$ and $h_\mu(x)$ are our unknown functions that are approximately piecewise constant. In two dimensions, this method produces two equations that we can solve directly to find $h_\lambda(x)$ and $h_\mu(x)$. For problems in three dimensions, the system will be overdetermined and can be solved using least squares.

Now that we have proposed functions that are approximately piecewise constant and contain both the coefficient values and the interface location, we need a method to extract these data, which we discuss in the next section.

4. Piecewise Constant Segmentation Methods

The problem of obtaining a segmentation of some given data that can be well approximated by a piecewise constant function has been well studied in the image processing literature. In our case, any suitable method could be applied to h_{pe} or h_λ and h_μ. We are going to focus on variational methods that have fast implementation methods available. However, other approaches would also produce viable results, including graph cuts [20], Markov random fields [42], and watershed algorithms [45], to name a few. We will now discuss the two variational methods used in this paper in detail.

4.1. Region Based Segmentation.

The first class of algorithms we look at are those based on the Mumford-Shah segmentation problem [44]. In particular, the Active Contours without Edges (ACWE) algorithm [16] solves this problem by finding the best piecewise constant approximation to the function over the domain,

$$\min_{\Gamma, c_1, c_2} Length(\Gamma) + \omega \int_{\Omega_1} (c_1 - f)^2 + \omega \int_{\Omega_2} (c_2 - f)^2 \tag{9}$$

where f is the function we are trying to approximate, ω is a constant that controls the scale of the features we want to find, and c_1 and c_2 are the values of the piecewise constant approximation in the two regions Ω_1 and Ω_2. In [16], the authors computed a curve that minimizes this energy via the gradient flow

$$\frac{\partial u}{\partial t} = H'_\epsilon(u)\left(\nabla \cdot \frac{\nabla u}{|\nabla u|} - \omega\left((c_1 - f)^2 - (c_2 - f)^2\right)\right) \tag{10}$$

where u is a level set function and H_ϵ is a C^∞ regularization of the Heaviside function, for a fixed c_1 and c_2.

The Globally Convex Segmentation (GCS) method proposed by Chan, Esedoglu, and Nikolova [15] modifies ACWE to be a globally convex minimization problem. This method starts from the observation that the steady state solution of (10) is the same as the steady state solution of

$$\frac{\partial u}{\partial t} = \nabla \cdot \frac{\nabla u}{|\nabla u|} - \omega \left((c_1 - f)^2 - (c_2 - f)^2\right) \tag{11}$$

which corresponds to a gradient descent for minimizing

$$E(u) = |\nabla u|_1 + \omega \langle u, r \rangle \tag{12}$$

where $r = (c_1 - f)^2 - (c_2 - f)^2$. In order to ensure that a global minimum to this problem is well-defined, we have to restrict the solution to lie in a specified interval. The final minimization problem is then

$$\min_{0 \le u \le 1} |\nabla u|_1 + \omega \langle u, r \rangle. \tag{13}$$

To find the two regions of the segmentation, we simply threshold

$$\Omega_1 = \{x : u(x) > a\} \tag{14}$$

for some $a \in (0, 1)$ and $\Omega_2 = \Omega_1^c \cap \Omega$. This minimization problem is now in a form where we can apply the split Bregman algorithm [25] as described in [24] to obtain a fast solver for this segmentation problem. This is accomplished by introducing an auxiliary variable $\vec{d} \leftarrow \nabla u$ and then approximately enforcing this equality constraint through a quadratic penalty term,

$$(u^*, \vec{d}^*) = \arg \min_{0 \le u \le 1, \vec{d}} |\vec{d}|_1 + \omega \langle u, r \rangle + \frac{\eta}{2} \|\vec{d} - \nabla u\|^2. \tag{15}$$

The equality constraint is then enforced exactly by applying Bregman iteration to (15), which results in the following sequence of optimization problems:

$$(u^{k+1}, \vec{d}^{k+1}) = \arg \min_{0 \le u \le 1, \vec{d}} |\vec{d}|_1 + \omega \langle u, r \rangle + \frac{\eta}{2} \|\vec{d} - \nabla u - \vec{b}^k\|^2, \tag{16}$$

$$\vec{b}^{k+1} = \vec{b}^k + \nabla u^k - \vec{d}^k. \tag{17}$$

The iterates u^{k+1} and $\vec{d}^{k+1}$ can be found by taking a single Gauss-Seidel iteration of

$$\Delta u = \frac{\omega}{\eta} r + \nabla \cdot (\vec{d} - \vec{b}), \text{ when } 0 < u < 1 \tag{18}$$

and solving

$$\vec{d}^{k+1} = shrink(\vec{b}^k + \nabla u^{k+1}, 1/\eta) \tag{19}$$

where the shrink operator is defined at each point $\gamma \in \Omega$ as

$$shrink(\vec{z}, \rho)_\gamma = \max\{\|\vec{z}_\gamma\| - \rho, 0\} \frac{\vec{z}_\gamma}{\|\vec{z}_\gamma\|}. \tag{20}$$

4.2. **Geodesic Active Contours.** Another class of segmentation algorithms are those that divide the image into regions by looking for the boundaries between objects. This is generally accomplished by using an edge stopping function that is computed from the gradient of the given data. Examples of this type of approach include snakes [35] and Geodesic Active Contours (GAC) [10]. The GAC model proposed by Caselles, Kimmel, and Sapiro [10] obtains solutions to this problem by solving

$$\min_{\Gamma} \int_{\Gamma} g(\nabla f) ds, \tag{21}$$

where Γ is a closed curve representing the boundary of the regions in the domain and g is an edge detecting function. A commonly used edge detector (and the one we will use in our examples) is

$$g(\xi) = \frac{1}{1+\tau|\xi|^2}. \tag{22}$$

with $\tau \geq 0$. Using a level set function, ϕ, to represent the curve Γ, solutions to (21) can be found by solving

$$\frac{\partial \phi}{\partial t} = \left(g\nabla \cdot \frac{\nabla \phi}{|\nabla \phi|} - \langle \nabla g, \nabla \phi \rangle \right) |\nabla \phi|. \tag{23}$$

In [7], the authors show how to obtain a convex variational form of GAC based on work by Chambolle on mean curvature motion [12] that allows for implicit time stepping in the evolution of the curve. The resulting minimization problem has the form

$$u^* = \min_u |\nabla u|_g + \frac{1}{2h}\|u - d_\Gamma\|^2 \tag{24}$$

where $|\cdot|_g = g|\cdot|_1$ is the weighted TV norm, d_Γ is a signed distance function representation of the curve Γ, and h corresponds to a time step for evolving the contour. To find the solution to the GAC model, we have to solve this minimization problem repeatedly, computing a signed distance function between each iteration with a method such as fast sweeping [61]. As before, we now have a model to which we can apply the split Bregman algorithm to obtain a fast solver for the segmentation. In this case, the sequence of minimization problems we need to solve has the form

$$(u^k, \vec{d}^k) = \arg\min_{u,\vec{d}} |\vec{d}|_g + \frac{1}{2h}\|u - d_\Gamma^k\| + \frac{\eta}{2}\|\vec{d} - \nabla u - \vec{b}^k\| \tag{25}$$

$$\vec{b}^{k+1} = \vec{b}^k + \nabla u^k - \vec{d}^k \tag{26}$$

where we alternate solving for u^k by taking one iteration of Gauss-Seidel on the system

$$\left(\frac{1}{h}I - \eta\Delta\right) u = \frac{1}{h} d_\Gamma^k + \eta\nabla \cdot (\vec{b} - \vec{d}) \tag{27}$$

and solving for $\vec{d}^k$ via the shrink operator

$$\vec{d}^k = shrink(\nabla u + \vec{b}, 1/\eta). \tag{28}$$

After solving for u^* in equation (24), we set d_Γ^{k+1} to be a signed distance function computed from u^* and then continue iterating the GAC model until it has converged.

Combining one of these two segmentation approaches with the formulae we derived in §3 for $h_{pe}(x)$, $h_\lambda(x)$, and $h_\mu(x)$, we now have a complete system for solving for the coefficients and

interface from solution data to Poisson's equation and linear elasticity. In the next section we show results of applying this process.

5. Numerical Experiments

We now demonstrate the algorithm on examples from Poisson's equation and linear elasticity in two dimensions, Poisson's equation in three dimensions, and a two-dimensional Poisson's equation example with noise. We also show a comparison of our method against more standard, variational techniques. All examples use the GCS approach described in §4.1 unless noted otherwise. An explicit choice of smoother S as mentioned in §3 is only necessary in examples with high levels of noise. In all other cases, the approximations to the differential operators are sufficiently smooth to produce reasonable results.

5.1. **Experiments in Two Dimensions.** For our first example we recover the interface and coefficients from data that are a solution to Poisson's equation on the domain $[0,1] \times [0,1]$ with zero Dirichlet boundary conditions and a right hand side of $f = 1$. The coefficients for the PDE were chosen to be $\beta_1 = 8$ and $\beta_2 = 1.5$. With $\omega = 1$ in the GCS algorithm, we find the two recovered regions shown in Figure 2. The coefficients in the two regions were found to be $\hat{\beta}_1 = 7.979$ and $\hat{\beta}_2 = 1.475$ corresponding to a relative error of about .3% in β_1 and 1.7% in β_2.

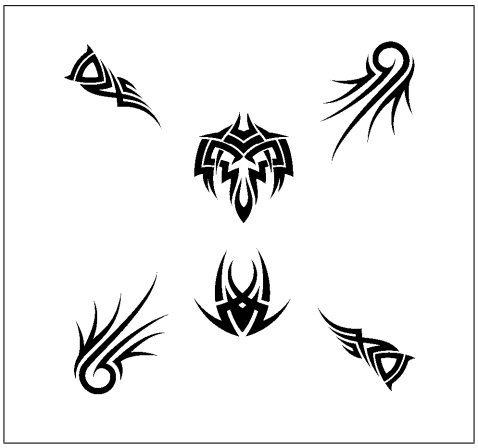

Figure 2. Recovered regions from Poisson's Equation example. Domain has 2400×2400 nodes.

Next we run an example where the given data are a solution to the equations of linear elasticity on $[0,1] \times [0,1]$ with free boundaries on the top and bottom and Dirichlet displacement data specified on the left and right edges of the square. The displacement vector is $-(.01, .015)$ on the left and $(.01, .015)$ on the right, resulting in a slight stretching and shearing of the material. Again, it is important to have a non-zero right hand side in order to obtain solutions to (8), so we set an external force vector of $\vec{f} = (1, 1)$ at each node. When generating the data, we used coefficients $(E_1, \nu_1) = (600, .33)$ and $(E_2, \nu_2) = (300, 0.28)$. The two recovered regions are shown in Figure 3, with $\omega = .1$ in the segmentation step. The recovered coefficients found in the two regions were $(\hat{E}_1, \hat{\nu}_1) = (599.98, 0.33)$ and $(\hat{E}_2, \hat{\nu}_2) = (289.12, 0.28)$ which corresponds to a relative error of less than 1% in every coefficient except for E_2 which has a relative error of 3.6%.

5.2. **Experiments in Three Dimensions.** We also demonstrate the ability to recover coefficients and the interface between the regions in three dimensions for Poisson's equation. In this case, our given data come from an exact solution to the PDE given by

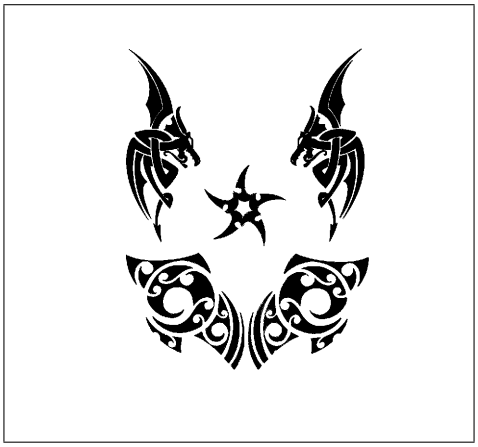

FIGURE 3. Recovered regions for linear elasticity. Domain has 1200×1200 nodes.

$$u(x,y,z) = \begin{cases} \frac{1}{6\beta_1}\left(x^2+y^2+z^2\right) & \text{for } (x,y,z) \in \Omega_1 \\ \frac{1}{6\beta_2}\left(x^2+y^2+z^2\right) & \text{for } (x,y,z) \in \Omega_2 \end{cases} \tag{29}$$

with appropriate Dirichlet boundary data given by the equation above and $f(x,y,z) = 1$. Using these data as input to our algorithm with $\beta_1 = 4$ and $\beta_2 = 22$, we are able to recover the interface shown in Figure 4 as well as coefficient values of $\hat{\beta}_1 = 3.96$ and $\hat{\beta}_2 = 22$. In the piecewise constant segmentation stage of the algorithm, we set $\omega = 1$. To demonstrate the computational efficiency of our approach, we also present some timings of our algorithm for the three dimensional problem at different resolutions, given in Table 1.

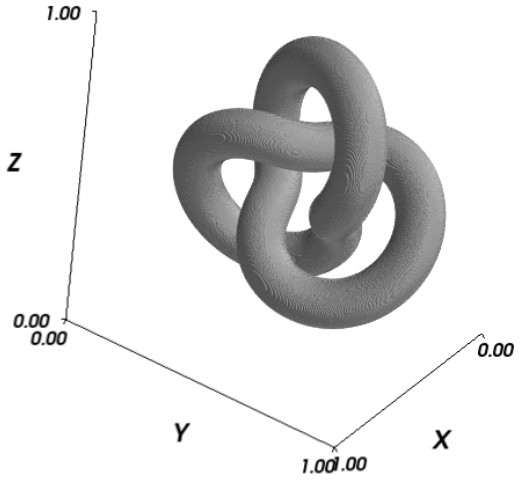

FIGURE 4. Recovered interface for the Poisson equation in 3d solved on a cube with 400 nodes in each dimension.

TABLE 1. Runtimes of the 3d solver for Poisson's equation at different grid resolutions. Tests were performed on an Intel Xeon X5365 3GHz processor. Runtime is the average of 10 simulations.

Grid Resolution	Runtime
128^3	0.616 s
256^3	5.237 s
512^3	43.616 s

5.3. **Experiments with Noise.** Next, we look at how our algorithm performs in the presence of noise and data corruption. We accomplish this by taking our given data, u_d, and adding Gaussian white noise that is determined relative to the maximum value in the given data,

$$u_d = u_d + n \tag{30}$$

where n is a vector of independent and identically distributed Gaussian random variables with zero mean and standard deviation $\alpha\|u_d\|_{L^\infty}$. For cases with high levels of noise, we find that the GAC method discussed in §4.2 performs better than the GCS method used for the previous examples. To compute the final coefficients in the two regions, we also find a median to be more robust than calculating a mean.

Results are shown in Figure 5 with the coefficient in the noise set to $\alpha = .01$. The data were generated using $\beta_1 = 12$ and $\beta_2 = 4$. The recovered coefficients were $\hat{\beta}_1 = 11.060$ and $\hat{\beta}_2 = 3.867$ corresponding to relative errors of 7.8% and 3.3%, respectively. A convolution with a Gaussian is performed prior to taking the Laplacian of the given data. The standard deviation of the Gaussian was chosen to be approximately $\sigma \approx 0.0857$.

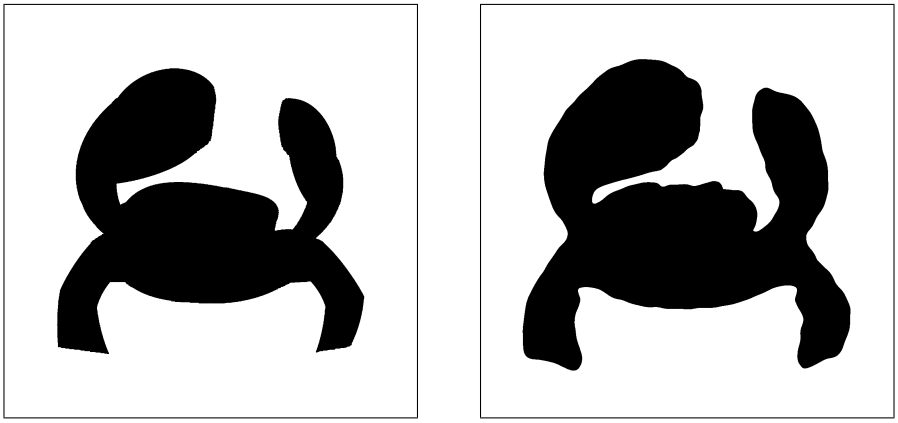

FIGURE 5. Original regions (left) and recovered noisy example (right) with 1400×1400 nodes. Original data was a solution to Poisson's equation.

5.4. **Comparison with Variational Methods.** Finally, we compare our method with more standard variational approaches [14, 19, 26, 46, 58, 59]. As mentioned in §2, these methods generally use a constrained optimization approach with output least squares and the augmented Lagrangian method to solve the optimization problem. We chose to compare to the method in [26] because we feel that it is representative of the general approach taken in the variational context.

We consider a linear elasticity example where the Lamé parameters are $E_1 = 200, \nu_1 = 0.28$, $E_2 = 117$, and $\nu_2 = 0.33$. The boundary displacement is $-(0.02, 0.01)$ on the left and $(0.02, 0.01)$

on the right, with free boundaries on the top and bottom. The variational algorithm has two control parameters and requires initial guesses for the coefficients and interface. These parameters are set to $w = 10^{-5}$ and $r = 0.004$. The initial guess for the interface is a three by three grid of circles and the coefficients are $E_1^0 = 230$, $\nu_1^0 = 0.3$, $E_2^0 = 80$, and $\nu_2^0 = .35$. For our method, the control parameter is set to $\omega = 1$. Coefficient results are summarized in Table 2 and the recovered regions are shown in Figure 6. Results are reported after 5000 iterations for the variational method.

We start by noting that variational methods require at least one linear system to be solved per iteration. For the method considered here, using a standard linear algebra package to solve the resulting equations with the conjugate gradient method results in a rather slow algorithm. The 5000 iterations used to compute the results in this section take approximately 33 hours on the same architecture used for the timing tests presented in Table 1. While this could definitely be improved through better choices of numerics, numerical tolerances, and initial guesses, this makes the method more complicated to implement and use in an efficient way. Our approach leads to an easy to implement, fast method. For this reason, the example used to compare the methods only has 256×256 nodes as the variational method cannot reasonably be run at higher resolutions. In the authors' experience, as the shape of the two regions becomes more complicated, it becomes increasingly difficult to find parameters for the variational approach that guarantee convergence in a timely fashion. This issue does not exist with the method discussed in this paper.

TABLE 2. Recovered coefficients and errors for our method and a variational approach [26].

	E_1	ν_1	E_2	ν_2
Exact Value	200	0.28	117	0.33
Our Method	197.093	0.282	114.975	0.318
Relative Error	1.5%	0.7%	1.7%	3.6%
Variational Method	208.752	0.2798	122.196	0.3299
Relative Error	4.4%	0.07%	4.4%	0.03%

6. Conclusion

In this paper we presented a fast, non-variational method for solving for both the interface and the coefficients of a solution to an embedded interface elliptic PDE with piecewise constant coefficients. Our approach works by building a function that is approximately piecewise constant and then using a suitable piecewise constant segmentation algorithm on that function. This results in an algorithm that has one parameter, corresponding to the scale of the segmentation. The method is also fast as demonstrated by the ability to solve high resolution problems in both two and three dimensions.

Acknowledgements

The regions in Figure 2 are a combination of images used with permission from `http://www.tribalshapes.com`. The regions in Figure 3 are a combination of images used with permission from `http://www.freetattoodesigns.org`. We would also like to thank Jeff Hellrung for providing the code to generate the level set for the trefoil knot used in the example shown in Figure 4.

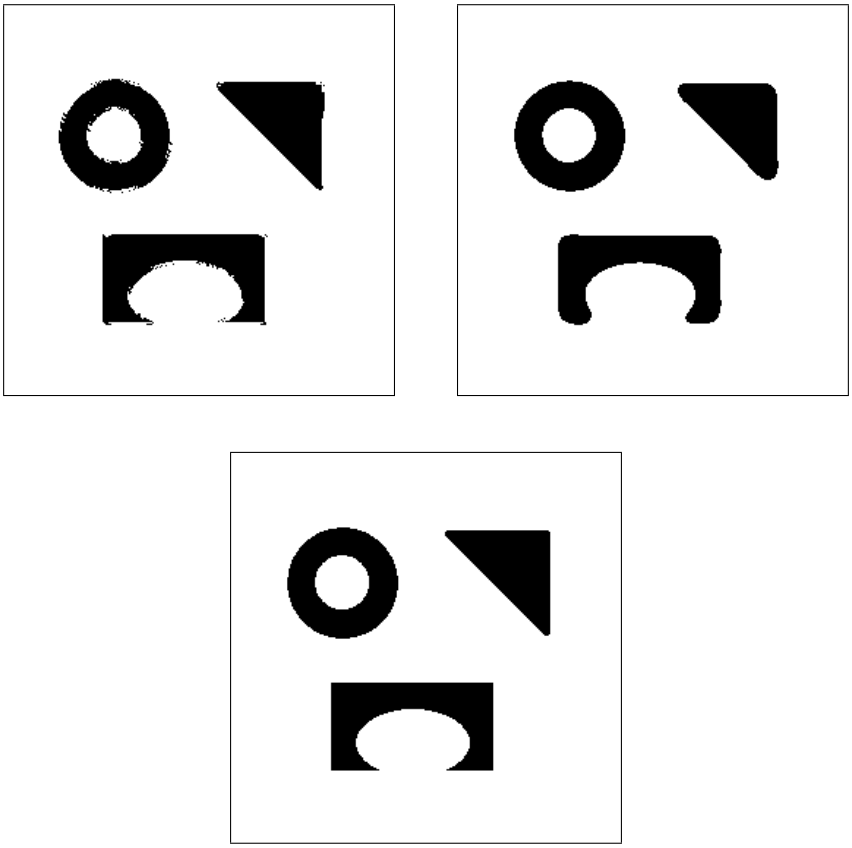

FIGURE 6. Comparison of our approach (top left) against a more standard variational method (top right). Original regions shown on the second row. Domain has 256×256 nodes.

References

[1] Grégoire Allaire, François Jouve, and Anca-Maria Toader. Structural optimization using sensitivity analysis and a level-set method. *Journal of Computational Physics*, 194(1):363 – 393, 2004.

[2] Diego Alvarez, Oliver Dorn, and Miguel Moscoso. A new level-set technique for the crack-detection problem. *PAMM*, 7(1):1081501–1081502, 2007.

[3] Hend Ben Ameur, Martin Burger, and Benjamin Hackl. Level set methods for geometric inverse problems in linear elasticity. *Inverse Problems*, 20(3):673–696, 2004.

[4] U. Ascher and E. Haber. Computational methods for large distributed parameter estimation problems with possible discontinuities. In *Symp. inverse problems, design and optimization*, pages 201–208, 2004.

[5] M.P. Bendsøe and O. Sigmund. *Topology optimization: theory, methods and applications*. Springer-Verlag, 2003.

[6] Liliana Borcea, Genetha Anne Gray, and Yin Zhang. Variationally constrained numerical solution of electrical impedance tomography. *Inverse Problems*, 19(5):1159–1184, 2003.

[7] X. Bresson and T.F. Chan. Active contours based on chambolle's mean curvature motion. In *Image Processing, 2007. ICIP 2007. IEEE International Conference on*, volume 1, pages I–33 – I–36, 2007.

[8] Martin Burger, Norayr Matevosyan, and Marie-Therese Wolfram. A level set based shape optimization method for an elliptic obstacle problem. *Mathematical Models and Methods in Applied Sciences*, 21(4):619–649, 2011.

[9] Martin Burger and Stanley J. Osher. A survey on level set methods for inverse problems and optimal design. *European Journal of Applied Mathematics*, 16(02):263–301, 2005.

[10] Vicent Caselles, Ron Kimmel, and Guillermo Sapiro. Geodesic active contours. *International Journal of Computer Vision*, 22(1):61–79, 1997.

[11] Vivien Challis, Anthony Roberts, and Andrew Wilkins. Fracture resistance via topology optimization. *Structural and Multidisciplinary Optimization*, 36:263–271, 2008.

[12] A. Chambolle. An algorithm for mean curvature motion. *Interfaces and Free Boundaries*, 6(2):195–218, 2004.

[13] T.F. Chan and X.C. Tai. Identification of Discontinuous Coefficients in Elliptic Problems Using Total Variation Regularization. *SIAM Journal on Scientific Computing*, 25:881–904, 2003.

[14] T.F. Chan and X.C. Tai. Level set and total variation regularization for elliptic inverse problems with discontinunous coefficients. *Journal of Computational Physics*, 193:40–66, 2004.

[15] Tony Chan, Selim Esedoglu, and Mila Nikolova. Algorithms for finding global minimizers of image segmentation and denoising models. *SIAM Journal on Applied Mathematics*, 66:1632–1648, 2006.

[16] Tony Chan and Luminita Vese. Active contours without edges. *IEEE Transactions on Image Processing*, 10:266–277, 2001.

[17] Z. Chen and J. Zou. An augmented Lagrangian method for identifying discontinuous parameters in elliptic systems. *SIAM Journal on Control and Optimization*, 37(3):892–910, 1999.

[18] M. Cheney, D. Isaacson, and J.C. Newell. Electrical impedance tomography. *SIAM Review*, 41:85–101, 1999.

[19] A. DeCezaro, A. Leitão, and X.C. Tai. On multiple level-set regularization methods for inverse problems. *Inverse Problems*, 25(3):035004, 2009.

[20] Pedro F. Felzenszwalb and Daniel P. Huttenlocher. Efficient graph-based image segmentation. *International Journal of Computer Vision*, 59(2):167–181, 2004.

[21] M.S. Gockenbach, B. Jadamba, and A.A. Khan. Equation error approach for elliptic inverse problems with an application to the identification of Lamé parameters. *Inverse Problems in Science and Engineering*, 16(3):349–367, 2008.

[22] M.S. Gockenbach and A.A. Khan. An abstract framework for elliptic inverse problems: Part 1. an output least-squares approach. *Mathematics and Mechanics of Solids*, 12(3):259–276, 2007.

[23] M.S. Gockenbach and A.A. Khan. An Abstract Framework for Elliptic Inverse Problems: Part 2. An Augmented Lagrangian Approach. *Mathematics and Mechanics of Solids*, 14(6):517–539, 2009.

[24] Tom Goldstein, Xavier Bresson, and Stanley Osher. Geometric applications of the split bregman method: Segmentation and surface reconstruction. *Journal of Scientific Computing*, 45:272–293, 2010.

[25] Tom Goldstein and Stanley Osher. The split bregman method for l1-regularized problems. *SIAM Journal on Imaging Science*, 2(2):323–343, 2009.

[26] Jan Hegemann, Alejandro Cantarero, Casey L. Richardson, and Joseph M. Teran. An explicit update scheme for inverse parameter and interface estimation of piecewise constant, discountinuous coefficients in linear elliptic pdes. *Submitted*.

[27] Frank Hettlich and William Rundell. Iterative methods for the reconstruction of an inverse potential problem. *Inverse Problems*, 12(3):251–266, 1996.

[28] Frank Hettlich and William Rundell. Recovery of the support of a source term in an elliptic differential equation. *Inverse Problems*, 13(4):959–976, 1997.

[29] Frank Hettlich and William Rundell. The determination of a discontinuity in a conductivity from a single boundary measurement. *Inverse Problems*, 14(1):67–82, 1998.

[30] Cosmina Hogea, Christos Davatzikos, and George Biros. An image-driven parameter estimation problem for a reaction-diffusion glioma growth model with mass effects. *Journal of Mathematical Biology*, 56:793–825, 2008.
[31] K. Ito and K. Kunisch. The augmented Lagrangian method for parameter estimation in elliptic systems. *SIAM Journal on Control and Optimization*, 28:113, 1990.
[32] Kazufumi Ito, Karl Kunisch, and Zhilin Li. Level-set function approach to an inverse interface problem. *Inverse Problems*, 17(5):1225, 2001.
[33] B. Jadamba, A.A. Khan, and F. Raciti. On the inverse problem of identifying lamé coefficients in linear elasticity. *Computers & Mathematics with Applications*, 56(2):431 – 443, 2008.
[34] Lin Ji, Joyce R McLaughlin, Daniel Renzi, and Jeong-Rock Yoon. Interior elastodynamics inverse problems: shear wave speed reconstruction in transient elastography. *Inverse Problems*, 19(6):S1 – S29, 2003.
[35] Michael Kass, Andrew Witkin, and Demetri Terzopoulos. Snakes: Active contour models. *International Journal of Computer Vision*, 1(4):321–331, 1988.
[36] I. Knowles, T. Le, and A. Yan. On the recovery of multiple flow parameters from transient head data. *Journal of Computational and Applied Mathematics*, 169:1–15, 2004.
[37] Ian Knowles. Parameter identification for elliptic problems. *Journal of Computational and Applied Mathematics*, 131:175–194, 2001.
[38] V. Kolehmainen, S. R. Arridge, W. R. B. Lionheart, M. Vauhkonen, and J. P. Kaipio. Recovery of region boundaries of piecewise constant coefficients of an elliptic pde from boundary data. *Inverse Problems*, 15(5):1375–1391, 1999.
[39] K. Kunisch and X.C. Tai. Sequential and parallel splitting methods for bilinear control problems in Hilbert spaces. *SIAM Journal on Numerical Analysis*, 34(1):91–118, 1997.
[40] Karl Kunisch and Xiaosu Pan. Estimation of interfaces from boundary measurements. *SIAM Journal on Control and Optimization*, 32(6):1643–1674, 1994.
[41] Hae Sung Lee, Cheon Jong Park, and Hyun Woo Park. Identification of geometric shapes and material properties of inclusions in two-dimensional finite bodies by boundary parameterization. *Computer Methods in Applied Mechanics and Engineering*, 181(1-3):1 – 20, 2000.
[42] Jose L. Marroquin, Edgar Arce Santana, and Salvador Botello. Hidden markov measure field models for image segmentation. *IEEE Transactions on Pattern Analysis and Machine Intelligence*, 25(11):1380–1387, 2003.
[43] Joyce R. McLaughlin, Ning Zhang, and Armando Manduca. Calculating tissue shear modulus and pressure by 2d log-elastographic methods. *Inverse Problems*, 26(8):085007, 2010.
[44] David Mumford and Jayant Shah. Optimal approximation by piecewise smooth functions and associated variational problems. *Communications on Pure and Applied Mathematics*, 42:577–685, 1989.
[45] Laurent Najman and Michel Schmitt. Geodesic saliency of watershed contours and hierarchical segmentation. *IEEE Transactions on Pattern Analysis and Machine Intelligence*, 18(12), 1996.
[46] Lars Kristian Nielsen, Xue-Cheng Tai, Sigurd Ivar Aanonsen, and Magne Espedal. A binary level set model for elliptic inverse problems with discontinuous coefficients. *International Journal of Numerical Analysis and Modeling*, 4:74–99, 2007.
[47] Assad A. Oberai, Nachiket H. Gokhale, and Gonzalo R. Feijóo. Solution of inverse problems in elasticity imaging using the adjoint method. *Inverse Problems*, 19(2):297–313, 2003.
[48] Guillaume Odin, Charles Savoldelli, Pierre-Olivier Bouchard, and Yannick Tillier. Determination of young's modulus of mandibular bone using inverse analysis. *Medical Engineering & Physics*, 32(6):630 – 637, 2010.
[49] Stanley Osher and James A Sethian. Fronts propagating with curvature-dependent speed: Algorithms based on hamilton-jacobi formulations. *Journal of Computational Physics*, 79(1):12 – 49, 1988.
[50] Stanley J. Osher and Fadil Santosa. Level set methods for optimization problems involving geometry and constraints: I. frequencies of a two-density inhomogeneous drum. *Journal of Computational Physics*, 171(1):272 – 288, 2001.
[51] Mauro Perego, Alessandro Veneziani, and Christian Vergara. A variational approach for estimating the compliance of the cardiovascular tissue: An inverse fluid-structure interaction problem. *SIAM Journal on Scientific Computing*, 33(3):1181–1211, 2011.
[52] Anand P. Santhanam, Yugang Min, Sudhir P. Mudur, Abhinav Rastogi, Bari H. Ruddy, Amish Shah, Eduardo Divo, Alain Kassab, Jannick P. Rolland, and Patrick Kupelian. An inverse hyper-spherical harmonics-based formulation for reconstructing 3d volumetric lung deformations. *Comptes Rendus Mcanique*, 338(7-8):461 – 473, 2010.
[53] Fadil Santosa. A level-set approach for inverse problems involving obstacles. *ESAIM: Control, Optimisation and Calculus of Variations*, 1:17–33, 1996.
[54] D. S. Schnur and Nicholas Zabaras. An inverse method for determining elastic material properties and a material interface. *International Journal for Numerical Methods in Engineering*, 33(10):2039–2057, 1992.
[55] J.A. Sethian and Andreas Wiegmann. Structural boundary design via level set and immersed interface methods. *Journal of Computational Physics*, 163(2):489 – 528, 2000.

[56] Nariida C. Smith and Keeva Vozoff. Two-dimensional dc resistivity inversion for dipole-dipole data. *Geoscience and Remote Sensing, IEEE Transactions on*, GE-22(1):21 –28, 1984.
[57] M. Soleimani, W.R.B. Lionheart, and O. Dorn. Level set reconstruction of conductivity and permittivity from boundary electrical measurements using experimental data. *Inverse problems in science and engineering*, 14:103 – 210, 2006.
[58] Xue-Cheng Tai and Hongwei Li. A piecewise constant level set method for elliptic inverse problems. *Applied Numerical Mathematics*, 57(5-7):686 – 696, 2007.
[59] K. van den Doel, U. Ascher, and A. Leitão. Multiple level sets for piecewise constant surface reconstruction in highly ill-posed problems. *Journal of Scientific Computing*, 43:44–66, 2010.
[60] K. van den Doel and U.M. Ascher. On level set regularization for highly ill-posed distributed parameter estimation problems. *Journal of Computational Physics*, 216(2):707 – 723, 2006.
[61] H. Zhao. A fast sweeping method for eikonal equations. *Mathematics of Computation*, 74:603–628, 2005.